



*Supplement of*

**Development of a land–river–ocean coupled model for compound floods jointly caused by heavy rainfall and storm surges in large river delta regions**

**Anyifang Zhang and Xiping Yu**

*Correspondence to:* Xiping Yu (yuxp@sustech.edu.cn)

The copyright of individual parts of the supplement might differ from the article licence.

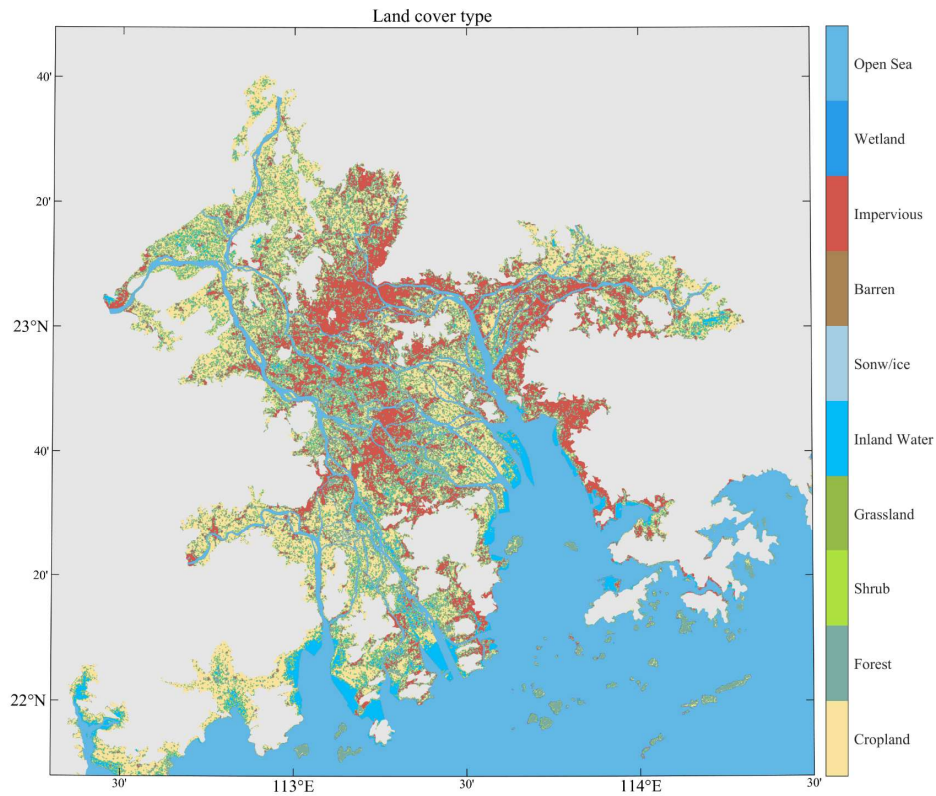


**Figure S1.** Distribution of land cover type in the Pearl River Delta region.

**Table S1.** Manning coefficient for different types of land cover.

Type of land cover	Manning coefficient
Open sea	0.01
Cropland	0.037
Forest	0.1
Shrub	0.05
Grassland	0.034
Inland Water	0.02
Snow	0.01
Barren	0.09
Impervious	0.15
Wetland	0.1

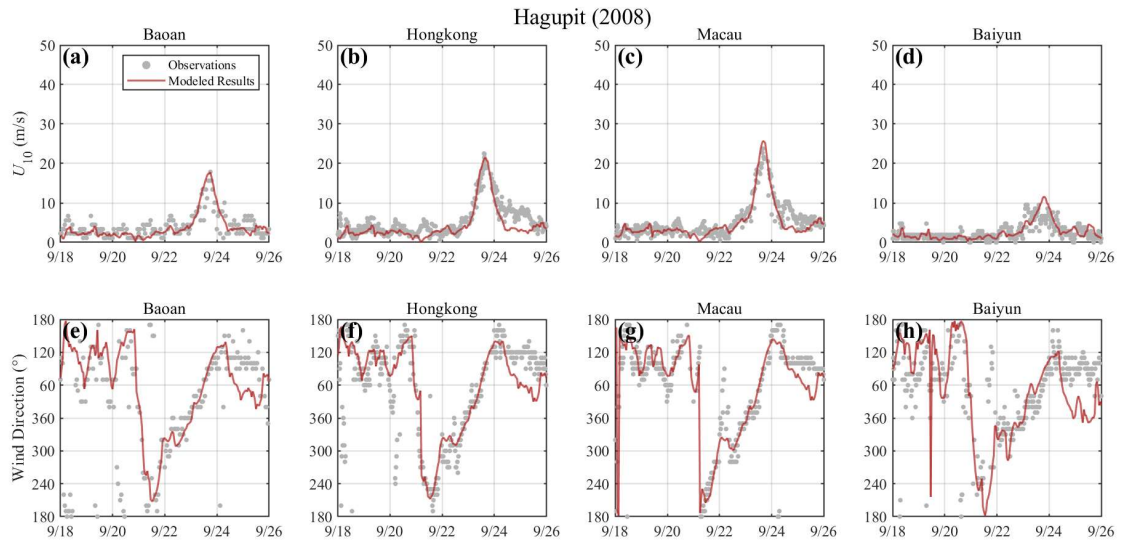


**Figure S2.** Comparison of computed and observed wind speed and wind direction during Typhoon Hagupit (2008) at four meteorological stations [I. Baoan, II. Hongkong, III. Macau, and IV. Baiyun].

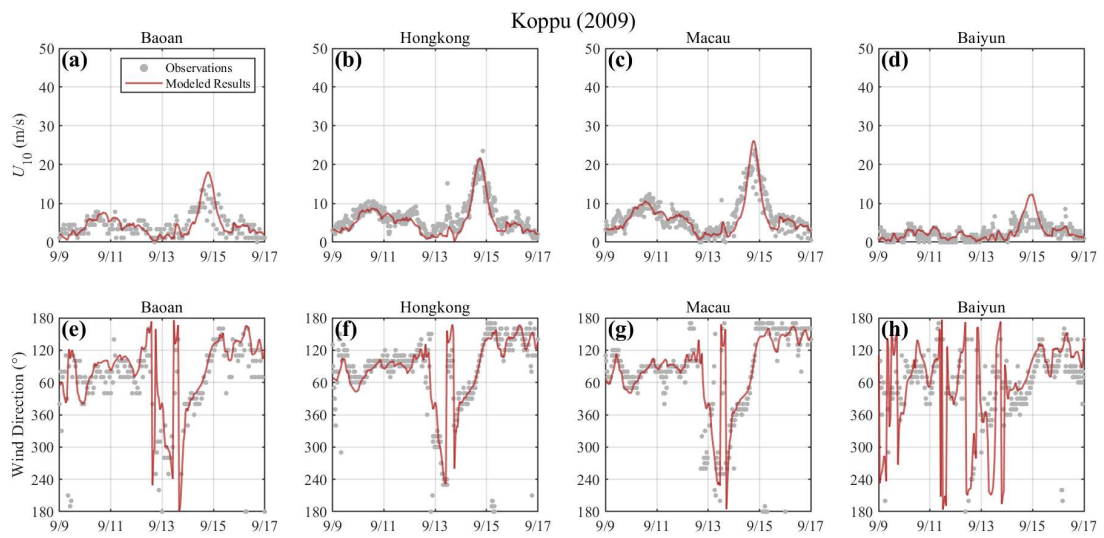


**Figure S3.** Same as **Figure S2** but during Typhoon Koppu (2009)

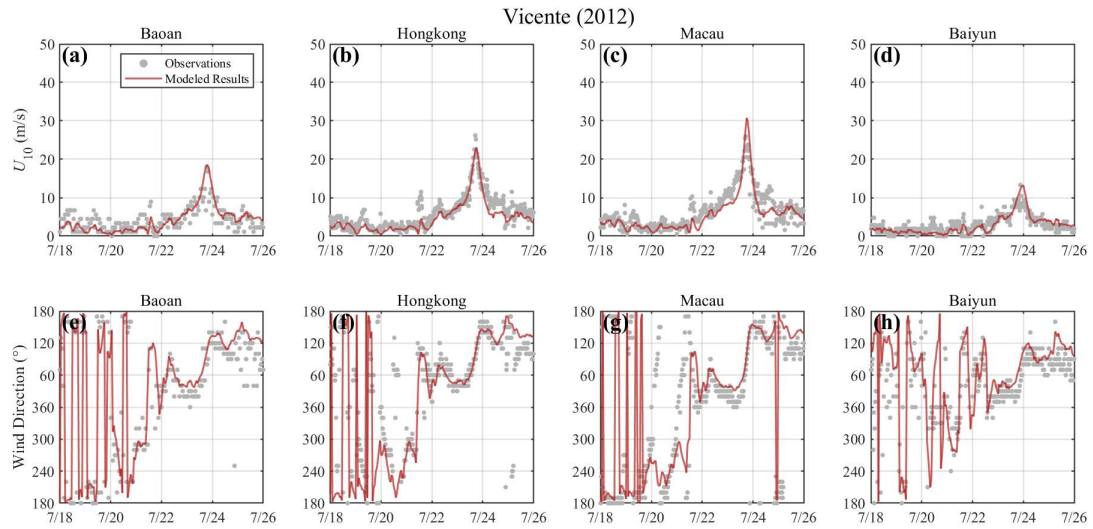


**Figure S4.** Same as **Figure S2** but during Typhoon Vicente (2012).

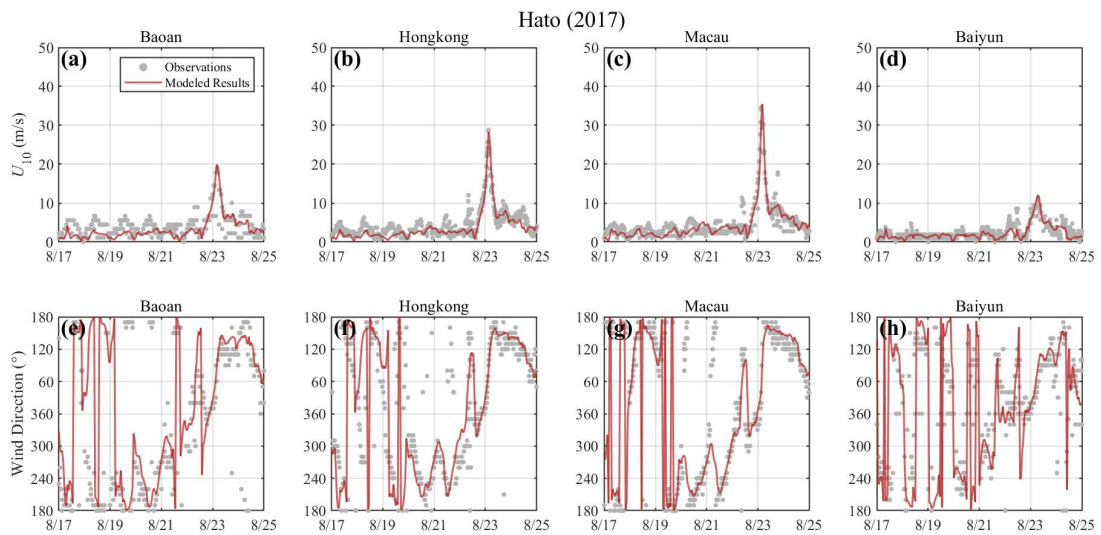


**Figure S5.** Same as **Figure S2** but during Typhoon Hato (2017).

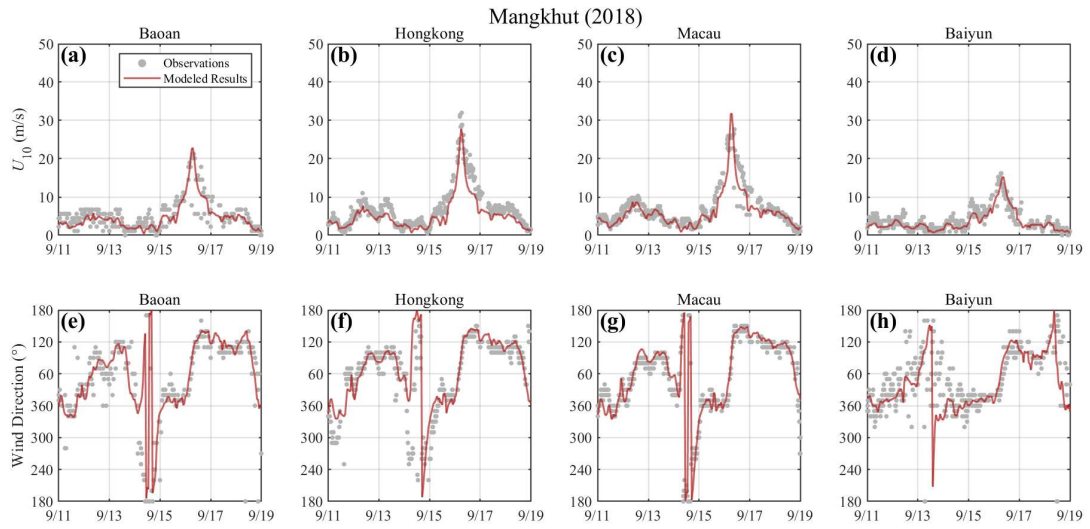


**Figure S6.** Same as **Figure S2** but during Typhoon Mangkhut (2018).

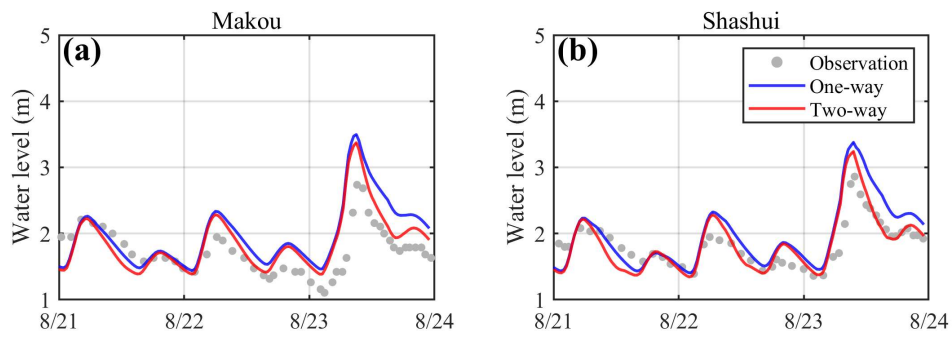


**Figure S7.** The simulated (solid lines) and observed (gray points) storm tides are compared at (a) Makou and (b) Sanshui stations.

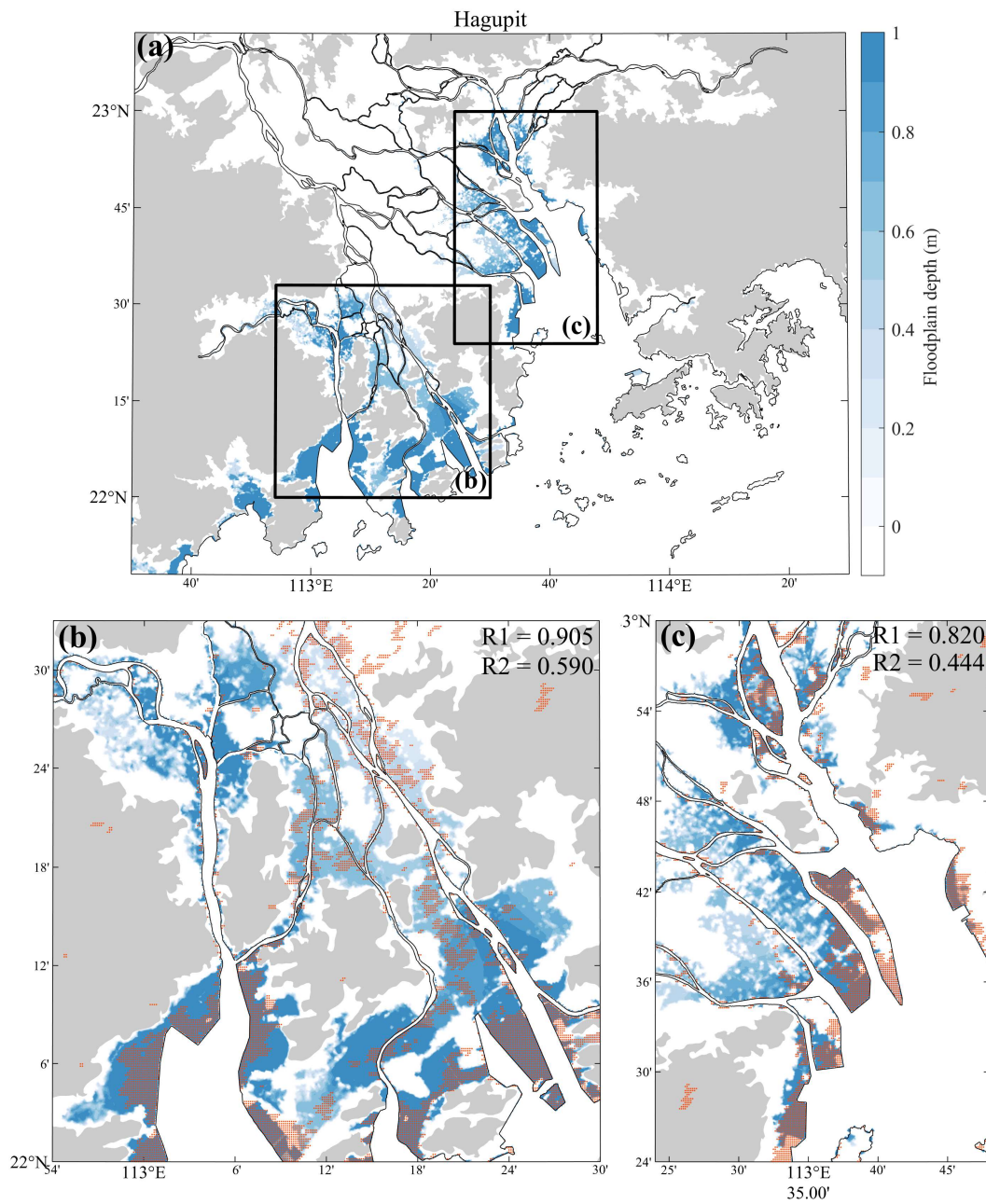


**Figure S8.** The contour plot (blue) of computed inundation depth caused by Typhoon Hagupit (2008). The orange dots are the inundation range estimated by MODIS datasets.

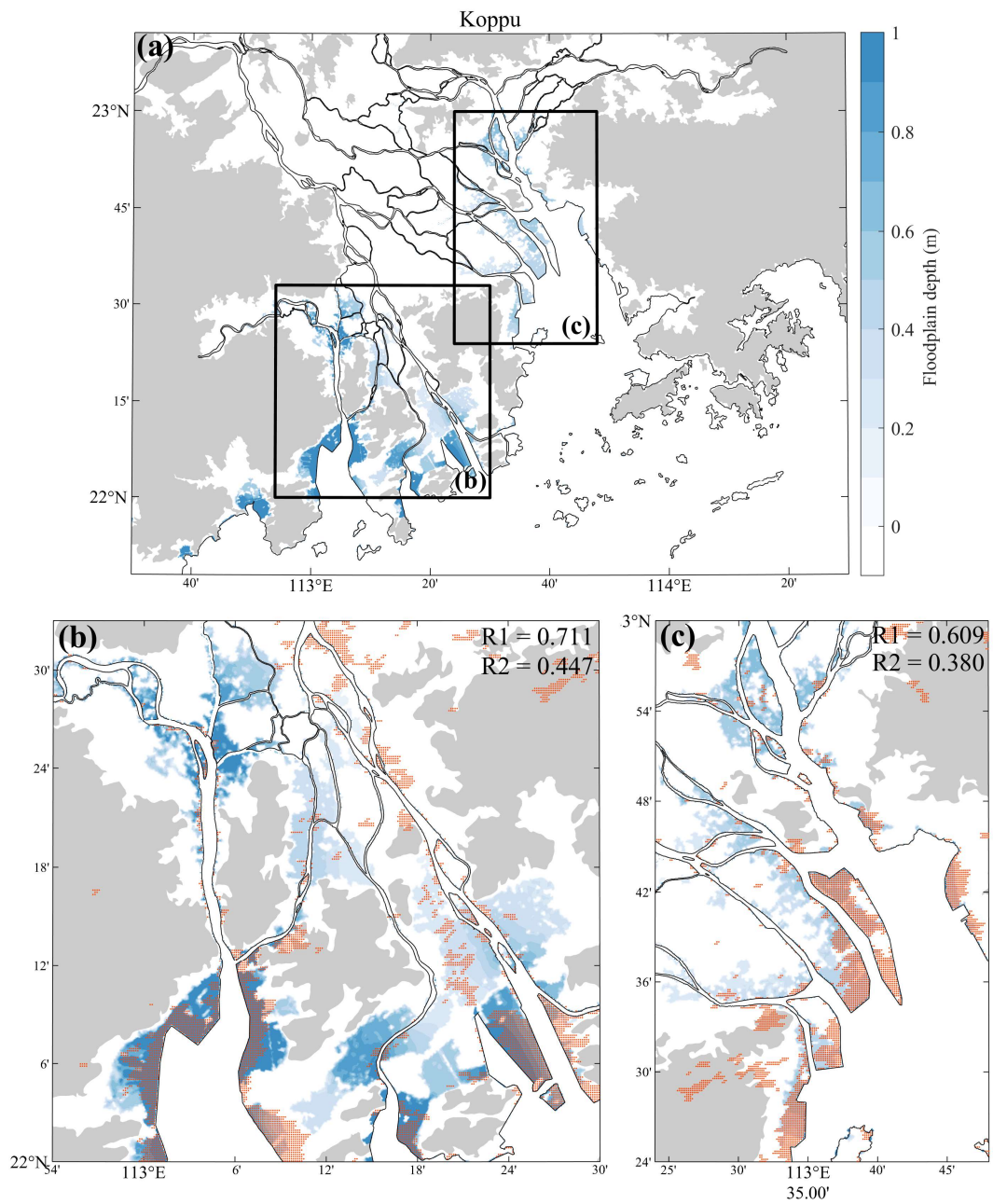


**Figure S9.** Same as **Figure S8** but caused by Typhoon Koppu (2009).

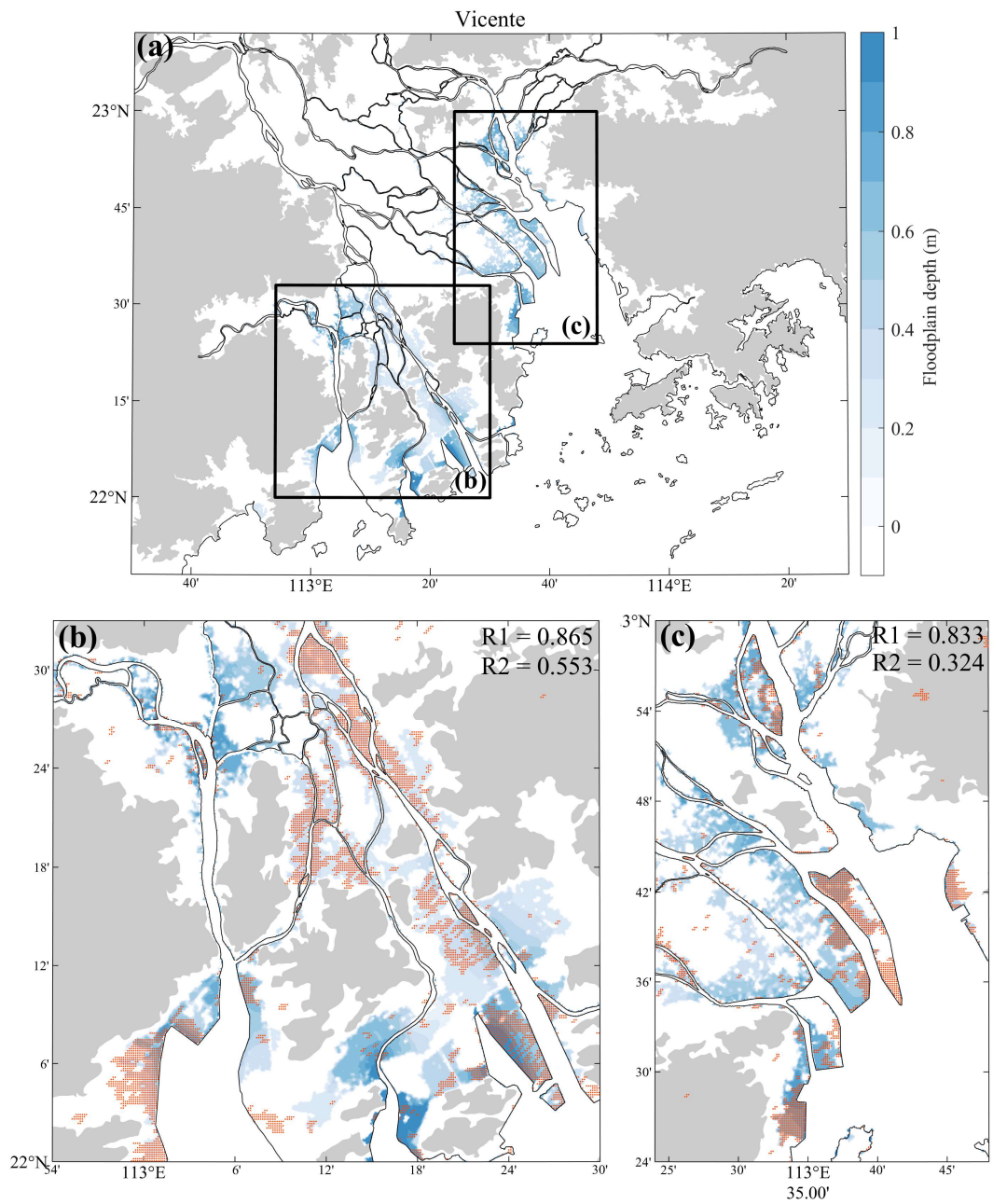


**Figure S10.** Same as **Figure S8** but caused by Typhoon Vicente (2012).

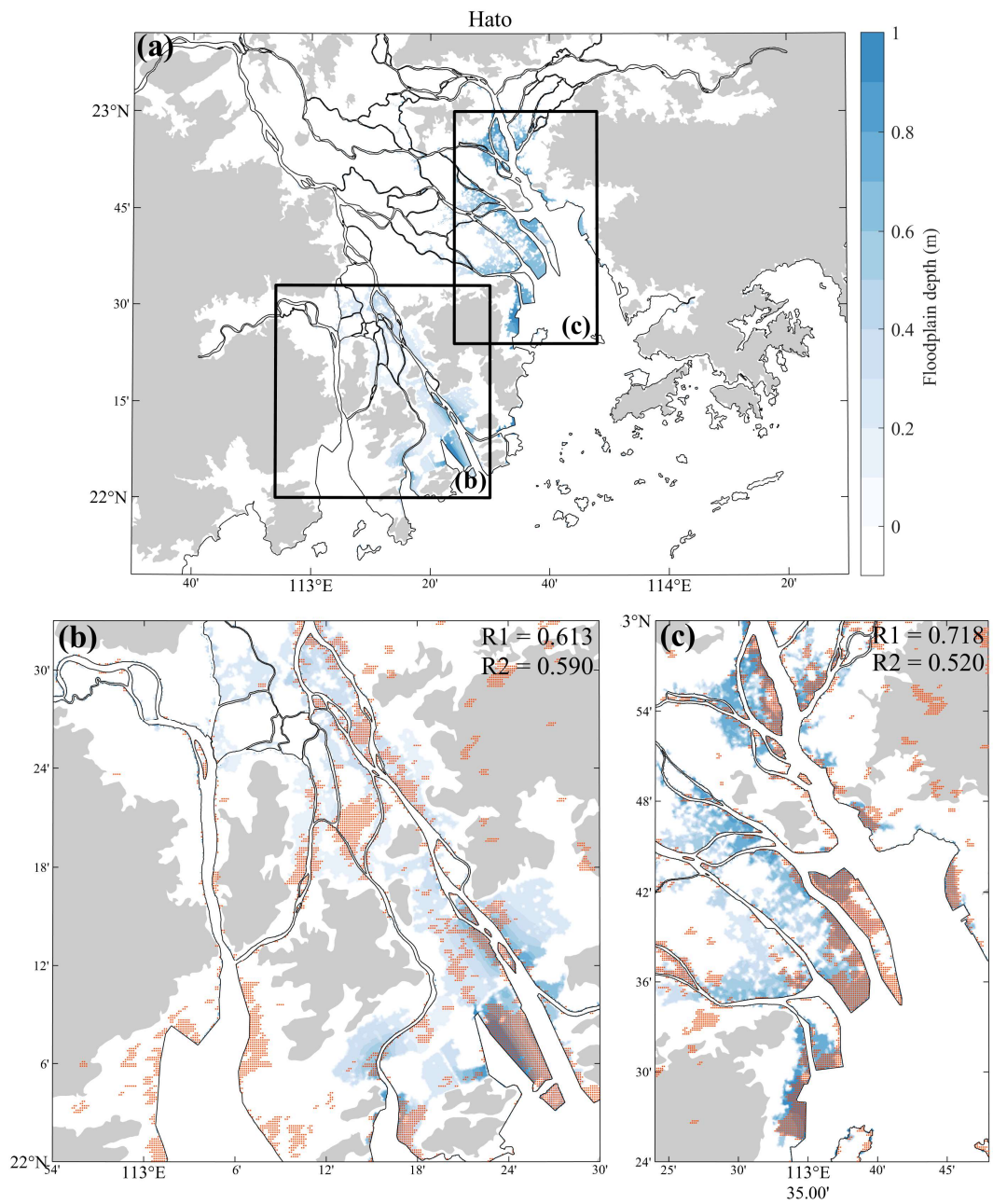


**Figure S11.** Same as **Figure S8** but for Typhoon Hato (2017).

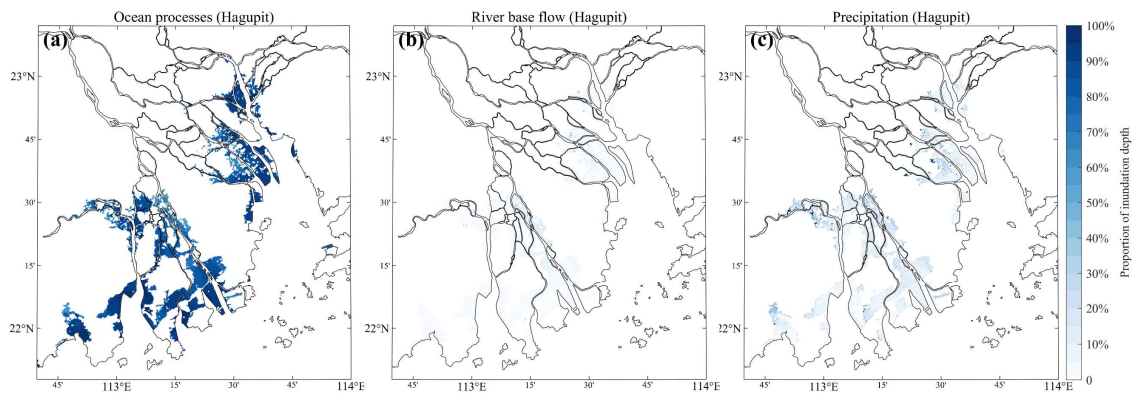


**Figure S12.** The distribution of inundation depth contributed by (a) the ocean processes, (b) the river base flow, and (c) the precipitation during Typhoon Hagupit (2008).

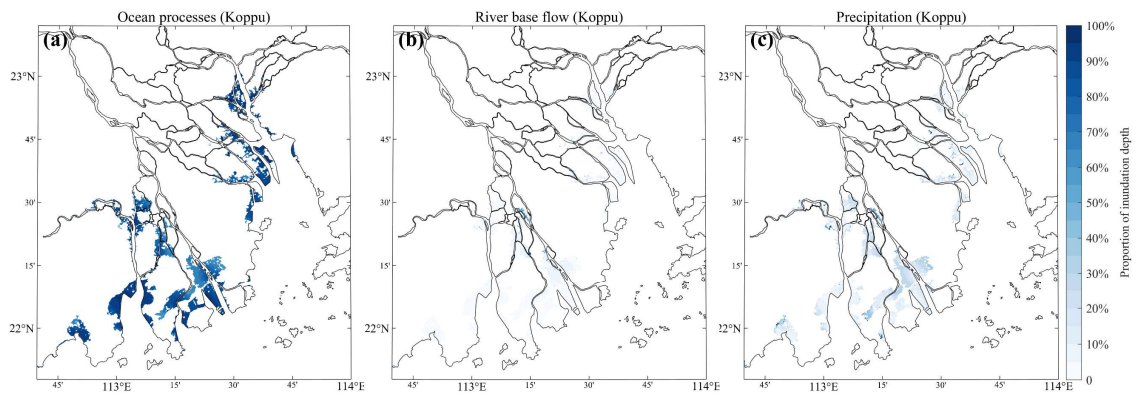


**Figure S13.** Same as Figure S12 but during Typhoon Koppu (2009).

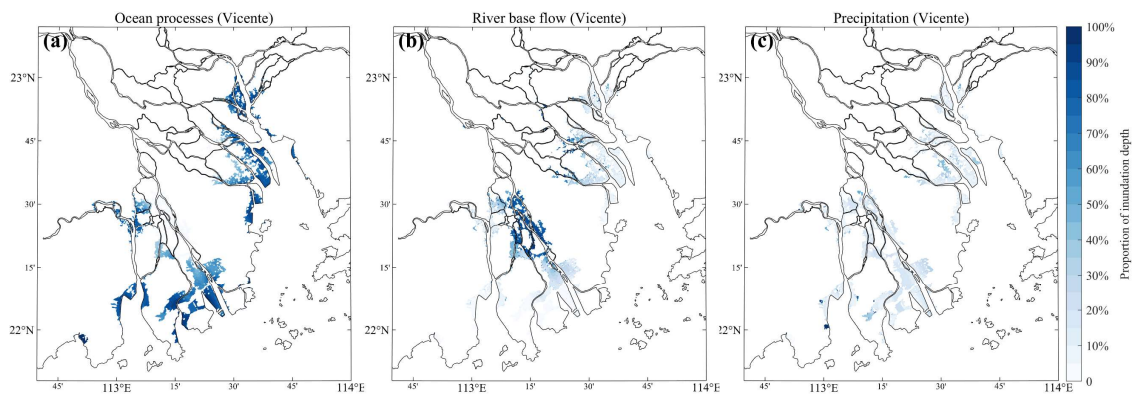


**Figure S14.** Same as **Figure S12** but during Typhoon Vicente (2012).

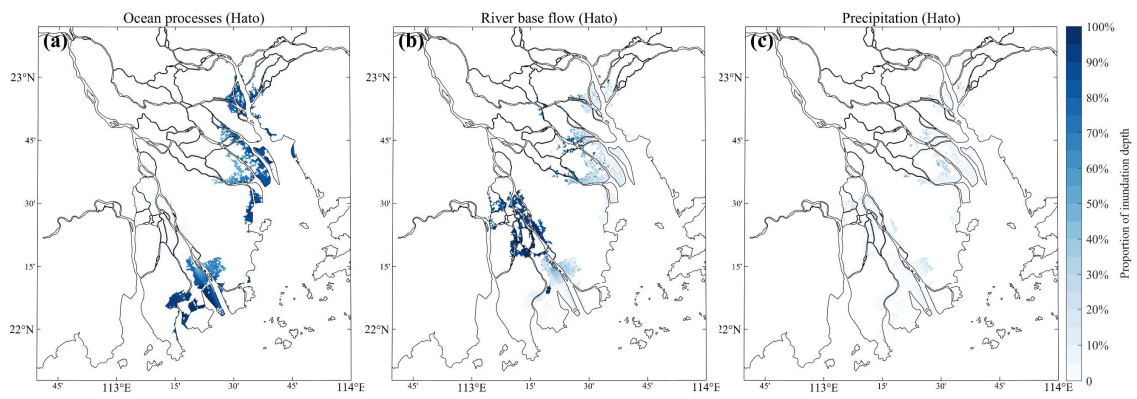


**Figure S15.** Same as **Figure S12** but during Typhoon Hato (2017).

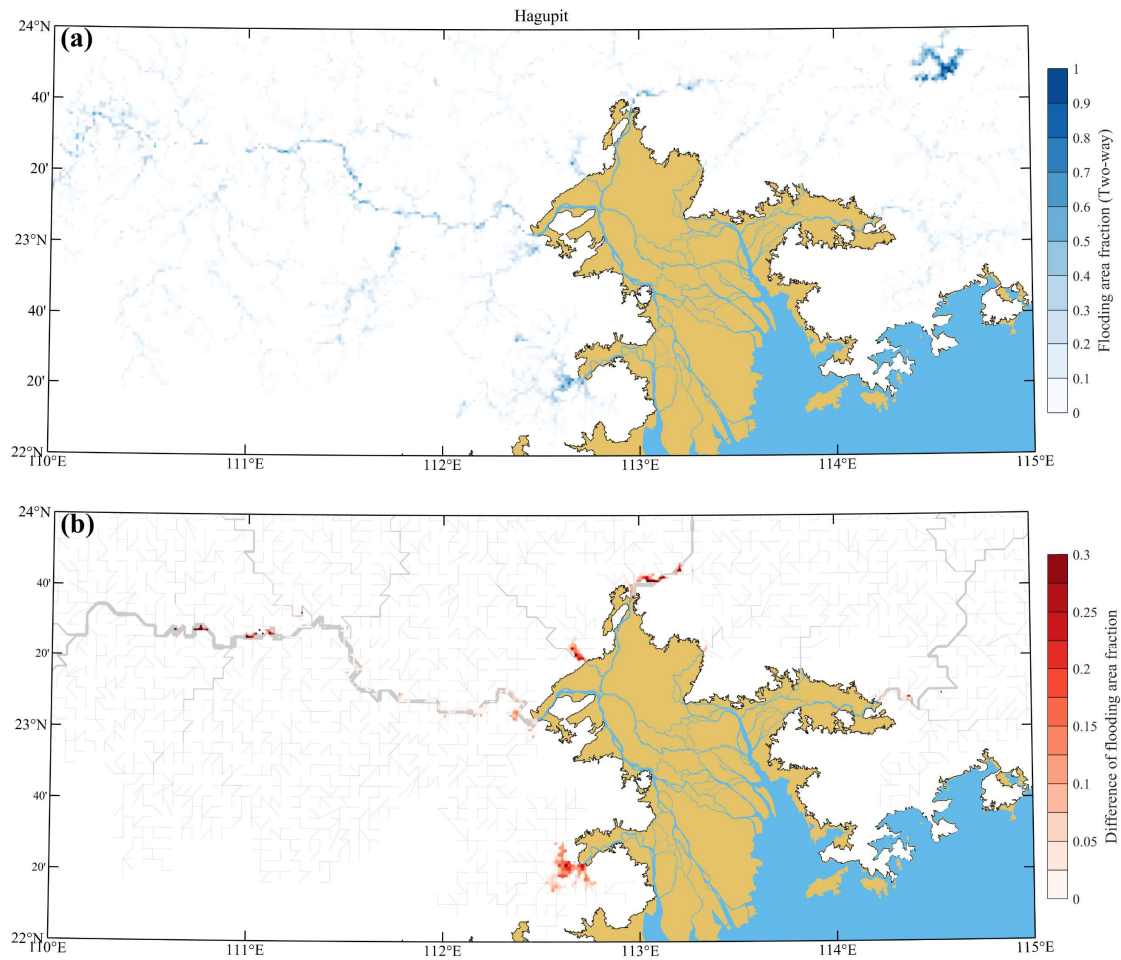


**Figure S16. (a)** The fraction of flooding area during Typhoon Hagupit (2008) estimated by the CaMa-flood model with two-way coupling approach. **(b)** The difference of the fraction of flooding area between the two-way and one-way coupling approaches. The river channels are marked with gray lines, with the width of the river channel indicated by the line thickness.

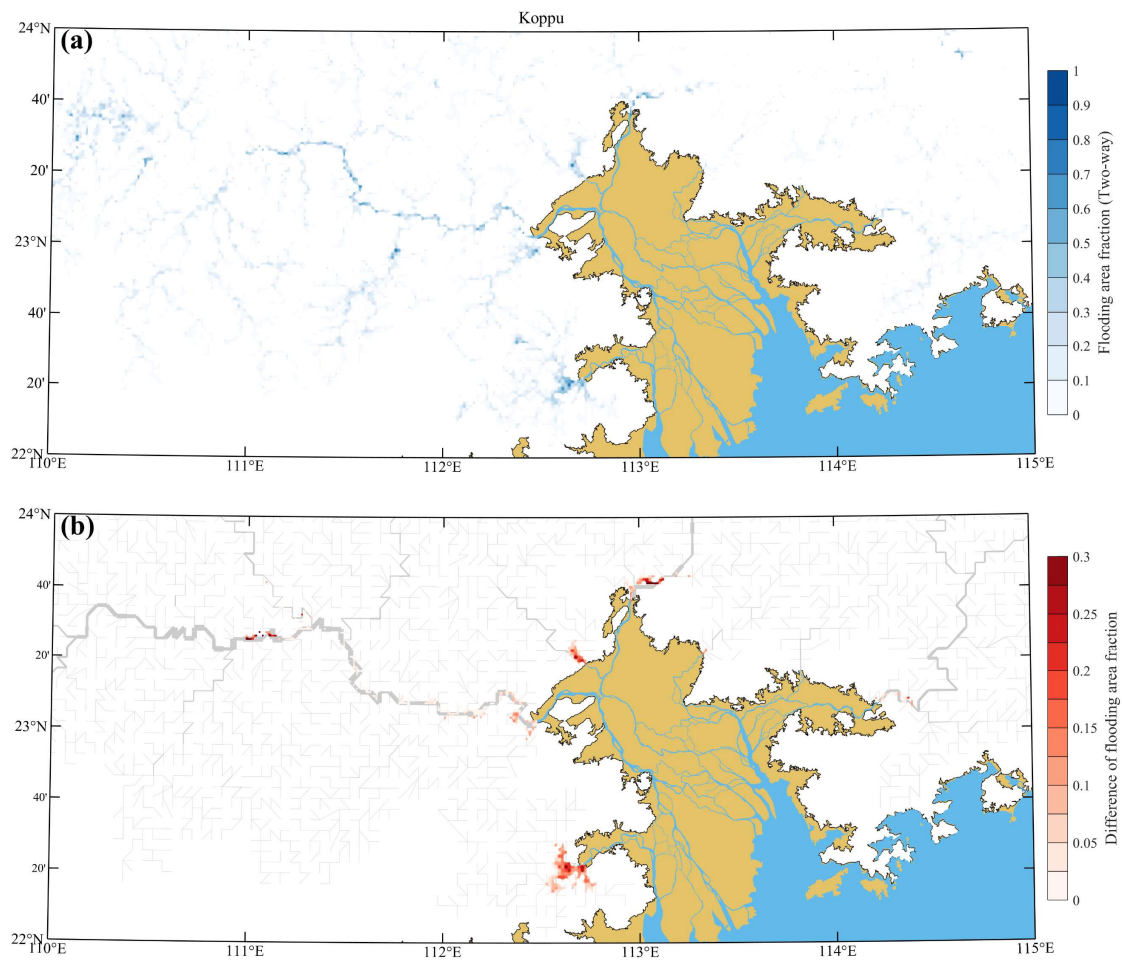


**Figure S17.** Same as **Figure S16** but during Typhoon Koppu (2009).

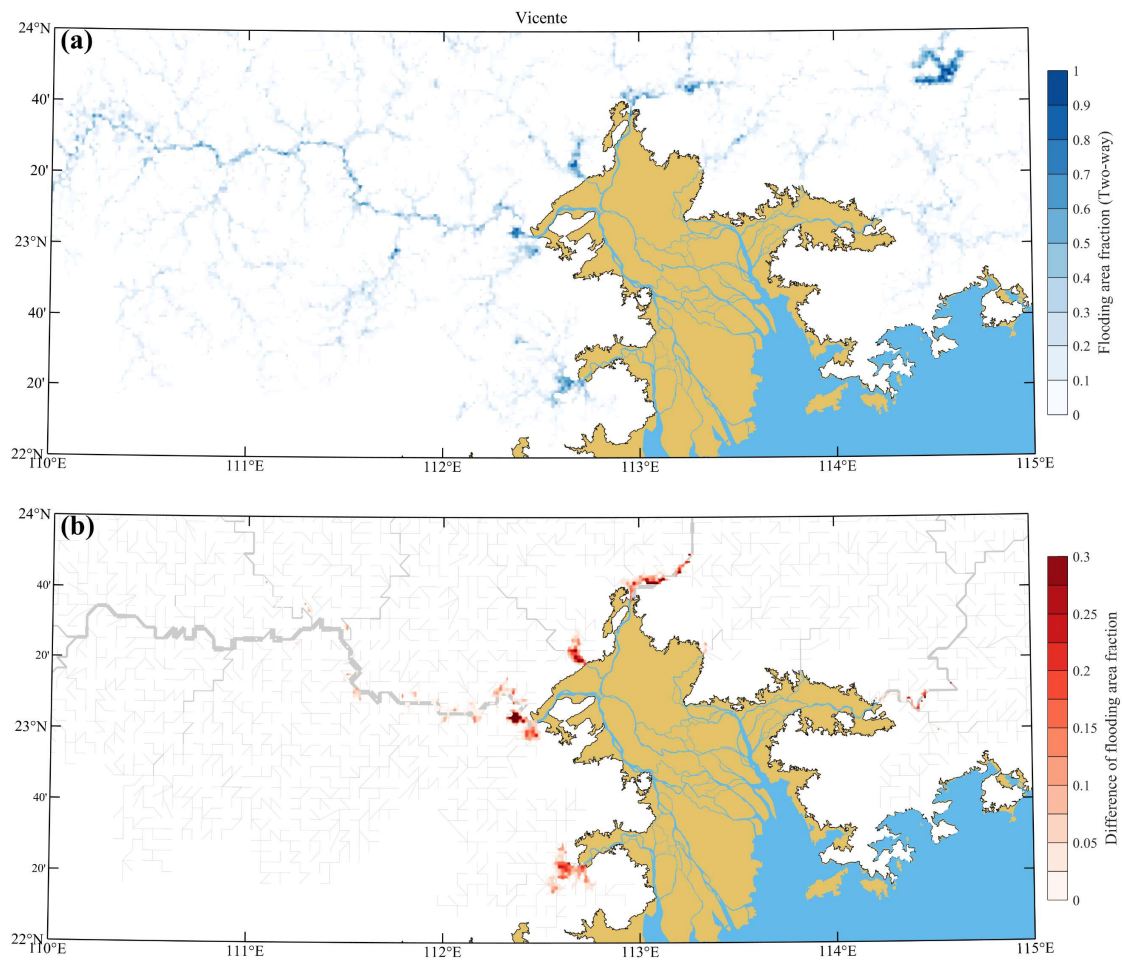


**Figure S18.** Same as **Figure S16** but during Typhoon Vicente (2012).

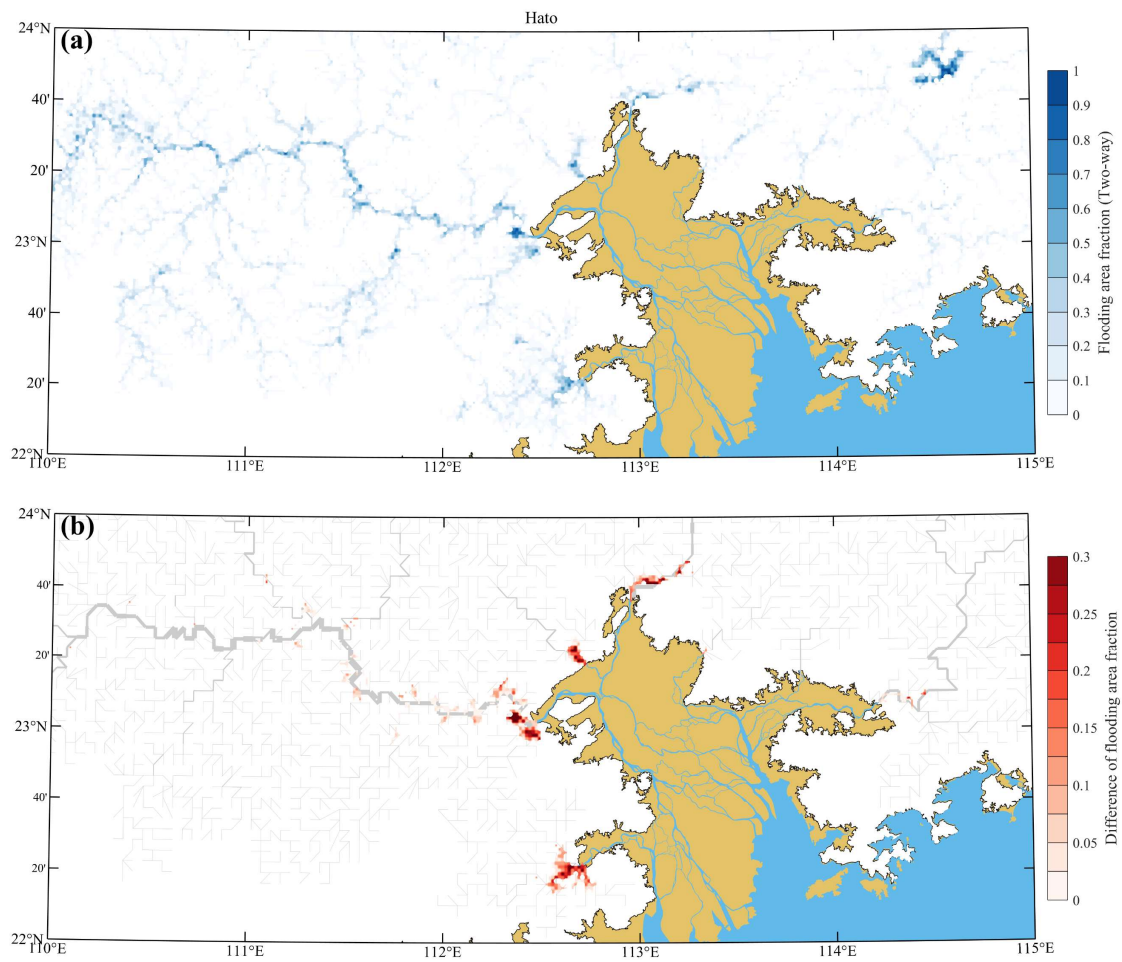


**Figure S19.** Same as **Figure S16** but for Typhoon Hato (2017).